Late Pleistocene changes in terrestrial biomarkers in sediments from the central Arctic Ocean

Masanobu Yamamoto [a*], Tatsufumi Okino [a], Saiko Sugisaki [b,c], Tatsuhiko Sakamoto [b]

[a] *Faculty of Environmental Earth Science, Hokkaido University, Kita-10, Nishi-5, Kita-ku, Sapporo 060-0810, Japan*

[b] *Institute for Research on Earth Evolution, Japan Agency for Marine-Earth Science and Technology, Natsushima-cho 2-15, Yokosuka 237-0061, Japan*

[c] *Department of Polar Science, The Graduate University for Advanced Studies, c/o National Institute of Polar Research, 9-10, Kaga 1-chome, Itabashi-ku, Tokyo 173-8515, Japan*

* Corresponding author. *E-mail address*: myama@ees.hokudai.ac.jp (M. Yamamoto).

Abstract

Biomarkers in Late Pleistocene sediments collected from the Integrated Ocean Drilling Program (IODP)-Arctic Coring Expedition (ACEX) Hole M0004C (central Arctic Ocean) were investigated. The major biomarkers are long-chain *n*-alkanes, *n*-fatty acids and *n*-alkan-1-ols, indicating fresh organic matter (OM) derived predominantly from higher plants. The dominance of terrestrial biomarkers is attributed to severe OM degradation caused by slow sedimentation in oxygen-rich benthic water and/or low primary production due to permanent sea-ice coverage. Hopanes, representing thermally altered OM, tend to be abundant in samples with abundant ice rafted debris (IRD). An

OM-rich dark grey layer deposited during marine isotope stage (MIS) 6 contains a significant amount of branched glycerol dialkyl glycerol tetraethers (branched GDGTs), suggesting ice erosion of organic-rich continental soil followed by transportation to the central Arctic by drifting ice. The labile–refractory index (i.e., the abundance ratio of long-chain *n*-alkan-1-ols to the sum of long-chain *n*-alkanes and long-chain *n*-alkan-1-ols) decreases above the dark grey layer, indicating that the OM became more refractory. This change suggests that coverage of the source region by OM-rich soil decreased because of extensive glacial erosion during MIS-6.

Keywords; Arctic, biomarker, glacial, IODP, ice rafted debris, paleoenvironment.

1. Introduction

Ice export from the Arctic to the Greenland Sea and North Atlantic Ocean is a potential factor in the formation of North Atlantic Deep Water (NADW; see Aagaard and Carmack, 1989; Darby et al., 2002). Its formation is a key process in thermohaline circulation and is linked to global climate change (Broecker, 1991). A complete understanding of the role of ice export from the Arctic requires records of iceberg and sea ice formation during past periods of climate change.

Icebergs and sea ice deposit ice-rafted debris (IRD), which has been used to reconstruct the Arctic's iceberg and sea ice formation history (e.g., Spielhagen et al., 2004). IRD source areas have been determined using mineral and chemical compositions (e.g., Stein et al., 1994; Darby et al., 2002). Organic geochemistry has also been applied in such studies; the amount and quality of bulk OM have been reported for sediment cores from the Amundsen Basin (Schubert and Stein, 1996) and the Siberian continental margins

(Stein et al., 2001, 2004; Bouscein et al., 2002). Biomarkers are now widely used as source-specific tracers in palaeoceanographic reconstruction, for example, in Holocene and late Pleistocene sequences of the Laptev and Kara Seas (Fahl and Stein, 1999; Stein et al., 2001).

Detrital matter is transported to the central Arctic Ocean by ice rafts. The Transpolar Drift transports sediment-laden “dirty” sea ice from the Laptev Sea, and eastward boundary currents along the northwestern Siberian margin and clockwise water circulation in the Beaufort gyre join with the Transpolar Drift (Gordienko and 1969; see Fig. 1) to contribute to mass transportation by ice-drift streams (Nürnberg et 1994). The central Arctic is therefore a suitable site for reconstructing past changes in transportation.

We examined late Pleistocene biomarker records collected from the Integrated Ocean Drilling Program (IODP)-Arctic Coring Expedition (ACEX) Hole M0004C in the Arctic Ocean, with the goal of understanding glacial-interglacial contrasts in biomarker composition in the Arctic Ocean and their relationship to late Pleistocene climate The results indicate an event of massive OM transport from the continent during Marine Isotope Stage (MIS) 6, which is discussed in relation to the expansion of the Eurasian Sheet.

2. Materials and methods

2.1. Samples

IODP Hole M0004C was drilled on the Lomonosov Ridge (87°52.065’N, 136°11.381’E) at a water depth of 1289 m in the central Arctic Ocean (Backman et al., 2006; Fig. 1). Sediments from Cores 302-M0004C-1H and -2H, taken 0–8.95 m below

the sediment surface (mbsf), comprise silty clay, silty mud and sandy mud with strong colour banding (Backman et al., 2006). Colour bands range in thickness from 2 to 50 cm and generally had sharp contacts. Bioturbation is minimal throughout the cores. Smear slide analysis indicated minor amounts of biogenic carbonate. Isolated pebbles (0.5–1.0 cm diam.) occur throughout the core. Cores were stored at ~5°C for two months. Samples of ca. 20 ml in volume were taken from the core and immediately frozen at -20°C at Bremen Core Repository. Samples were freeze-dried, mixed and split into aliquots.

2.2. Age–depth model

O'Regan et al. (2008) recently revised the composite depth scale for ACEX holes published by Backman et al. (2006). We used O'Regan et al.'s (2008) revised composite depth (rmcd) scale and their age–depth model (Fig. 2). The age-depth model was developed from three C-14 dates of planktonic foraminifera (6, 25, and 32 ka), two magnetic excursions (for Mono Lake and Laschamp [average age 38 ka], as reported by Lamgereis et al., 1997), a geomagnetic event (the Norwegian Greenland Sea event [55–66 ka] described by Nowaczyk and Frederichs, 1999), and seven tie points [79–338 ka] obtained from stratigraphic correlation of bulk density with nearby 96/12-PC (Jakobsson et al., 2001) and PS-2185-6 cores (Fütterer, 1992). According to this age–depth model, the sequence of the uppermost 6 m covers the last 300 ka (MIS-1 to MIS-8).

2.3. TOC measurement

Samples were analyzed for total organic carbon (TOC) using a LECO WR-112

carbon analyzer. The analyzer was attached to a halogen trap (antimony and potassium iodide). To remove carbonate carbon, the sample was acidified as follows: aliquots of ca. 0.5–0.8 g were soaked in 1 M HCl in a ceramic crucible overnight and then heated at 110°C for 3 h after adding more 1 M HCl. The sample was rinsed (x 2) to remove chlorides by adding distilled water and was again heated at 110°C for 3 h. The measurement precision was better than 0.01 wt%.

2.4. Ice rafted debris (IRD) count and grain-size analysis

The number of IRD particles (> 1 mm) was counted using an X-ray radiograph. The sand content (> 63 μm) was measured by sieving. Further details and description of the methods and results will be published elsewhere (Sakamoto et al., in preparation).

2.5. Low-molecular-weight lipid analysis

Lipids were extracted (x 2) from ca. 4 g of dried sediment using a DIONEX Accelerated Solvent Extractor ASE-200 at 100°C and 1000 psi for 10 min with 11 ml of CH_2Cl_2–CH_3OH (6:4) and then concentrated. The lipid extract was separated into four fractions using column chromatography (SiO_2 with 5% distilled water; i.d., 5.5 mm; length, 45 mm): F1 (hydrocarbons), 3ml hexane; F2 (aromatic hydrocarbons), 3 ml hexane-toluene (3:1); F3 (ketones), 4 ml toluene; F4 (polar compounds), 3 ml toluene–CH_3OH (3:1); *n*-$C_{24}D_{50}$ and *n*-$C_{36}H_{74}$ were added as internal standards to F1 and F3, respectively.

An aliquot of F4 was trans-esterified with 1 ml 5% HCl–CH_3OH at 60˚C for 12 h under N_2. The esterified lipids were supplemented with 2 ml distilled water and extracted (x 3) with toluene. The extract was back-washed (x 3) with distilled water,

passed through a short bed of Na_2SO_4, and separated into two fractions with SiO_2 column chromatography: F4-1 (acids), 4 ml toluene; F4-2 (alcohols), 3 ml toluene-CH_3OH (3:1); *n*-$C_{24}D_{50}$ was added as an internal standard to F4-1 and F4-2. Prior to gas chromatography (GC) analysis, F4-2 was silylated with BSTFA (*N*,*O*-bis(trimethylsilyl)trifluoroacetamide–pyridine (1:1) at 70˚C for 30 min.

Gas chromatography (GC) was conducted using a Hewlett Packard 5890 series II gas chromatograph with on-column injection and electronic pressure control systems, and a flame ionization detector (FID). Samples were dissolved in hexane. He was the carrier gas and the flow velocity was maintained at 30 cm/s. A Chrompack CP-Sil5CB column was used (length, 60 m; i.d., 0.25 mm; thickness, 0.25 μm). The oven temperature was programmed to rise from 70 to 130˚C at 20˚C/min, from 130 to 310˚C at 4˚C/min, and to hold at 310˚C for > 30 min. The standard deviations of five duplicate analyses averaged 7.5% of the concentration for each compound.

Gas chromatography-mass spectrometry (GC-MS) of F1, F3, F4-1 and F4-2 was conducted using a Hewlett Packard 5973 GC-mass selective detector with on-column injection and electronic pressure control systems, and a quadrupole mass spectrometer. The GC column and oven temperature and carrier pressure programmes were as described above. The mass spectrometer was run in full scan mode (*m/z* 50–650). Electron ionization (EI) spectra were obtained at 70 eV. Compound identification was achieved by comparing mass spectra and retention times with those of standards and published data.

2.6. Glycerol dialkyl glycerol tetraether (GDGT) analysis

An aliquot of F4 was dissolved in hexane–2-propanol (99:1). Glycerol dialkyl

glycerol tetraethers (GDGTs) were analyzed using high performance liquid chromatography-mass spectrometry (HPLC-MS) with an Agilent 1100 HPLC system connected to a Bruker Daltonics micrOTOF-HS time-of-flight mass spectrometer. Separation was conducted using a Prevail Cyano column (2.1 x 150 mm, 3μm; Alltech) and maintained at 30˚C following the method of Hopmans et al. (2000) and Schouten et al. (2007a). Conditions were: flow rate 0.2 ml/min, isocratic with 99% hexane and 1% 2-propanol for the first 5 min followed by a linear gradient to 1.8% 2-propanol over 45 min. Detection was achieved using atmospheric pressure, positive ion chemical ionization-mass spectrometry (APCI-MS). The spectrometer was run in full scan mode (*m/z* 500–1500). Compounds were identified by comparing mass spectra and retention times with those of GDGT standards (formed from the main phospholipids of *Thermoplasma acidophilum* via acid hydrolysis) and those in the literature (Hopmans et al., 2000). Quantification was achieved by integrating the summed peak areas in the $(M+H)^+$ and the isotopic $(M+H+1)^+$ ion traces and comparing these to an external calibration curve prepared using known amounts of the above-mentioned GDGT standard mixture.

3. Results

3.1. Biomarkers

Typical gas chromatograms of F1, F4-1 and F4-2 and LC/MS chromatograms of F-4 are shown in Figs. 3 and 4, respectively.

3.1.1. F1 fraction

N-alkanes occur as a major component of the F1 (hydrocarbon) fraction and show a unimodal distribution with a maximum at C_{29} (Fig. 3A). The odd/even carbon number

preference index (CPI) values of C_{24}-C_{34} homologues (Bray and Evans, 1961) vary between 3.1 and 7.1, with an average of 4.9 (Fig. 5F). Hopanes (C_{29}-C_{31}) in F1 comprise 17α(H),21β(H)-30-norhopane, 17α(H),21β(H)-hopane and 17β(H),21β(H)-homohopane (Fig. 3A). Homohopane 17α(H),21β(H), 17β(H),21α(H), and 22S isomers are absent. Neohop-13(18)-ene is found only in the core-top sample (0.1 rmcd). Olean-12-ene and olean-18-ene are also detected as minor compounds (Fig. 3A). Branched aliphatic alkanes with a quaternary substituted carbon atom (BAQCs) are detected in relatively high amounts and comprised 3,3-ethylmethylalkanes, 3,3,-dimethylalkanes, 5,5-diethylalkanes, 5,5-ethylmethylalkanes and some unidentified homologous series (Fig. 3A). The origin of BAQCs used to be unknown (Kenig et al., 2003), but recently they have been reported as contaminants from plastic bags (Grosjean and Logan, 2007). Because our samples were stored in plastic bags, they are likely contaminated.

3.2.2. F3 fraction

N-alkan-2-ones are a major component of the F3 and exhibit a unimodal distribution with a maximum at C_{27}. No long-chain alkenones are detected.

3.1.3. F4-1 fraction

Straight-chain fatty acids, which are detected as fatty acid-methyl esters, occur as a major component of the F4-1 and show a bimodal distribution with maxima at C_{18} and C_{26} (Fig. 3B). The even/odd CPI values of C_{23}–C_{33} homologues vary between 2.9 and 5.0, with an average of 3.7 (Fig. 5F). *Anteiso*-(C_{15} and C_{17}) and *iso*-fatty acids (C_{14}–C_{17}) are also detected as minor components (Fig. 3B). Monounsaturated *n*-C_{16} acids and mono- and di-unsaturated *n*-C_{18} acids are also detected (Fig. 3B). Di-unsaturated *n*-C_{18} acid is much less abundant than the mono-unsaturated (Fig. 5N).

3.1.4. F4-2 fraction

N-alkan-1-ols occur as a major component of the F4-2 and have a unimodal distribution maximizing at C_{26} (Fig. 3C). The even/odd CPI values of C_{23}–C_{33} homologues vary between 2.0 and 5.8, with an average of 4.7 (Fig. 5F). Hydroxy fatty acids with the OH group in the α, β, ω or (ω–1) positions are detected, and all show a similar homologous pattern with a maximizing at C_{24} or C_{26} (Fig. 3C). *N*-alkan-2-ols are present and show a unimodal distribution with a maximum at C_{29} (Fig. 3C). Cholesterol and β-sitosterol are detected as minor components (Fig. 3C).

3.1.5. High-molecular-weight lipids in the F4 fraction

LC/MS revealed that GDGTs are a major high-molecular-weight component of the F4 and comprise both isoprenoid and branched components. The isoprenoid GDGTs include cardarchaeol (GDGT-0), GDGT-1, GDGT-2, GDGT-3, and crenarchaeol. Whereas caldarchaeol and crenarchaeol are relatively abundant, caldarchaeol shows greater abundance than crenarchaeol in all but two samples (Fig. 4). Branched GDGTs make up a homologous series with four to six methyl groups (Hopmans et al., 2004; Fig. 4).

3.2. TOC content

The TOC content varies between 0.07 and 0.86%, with an average of 0.19%. A high content (0.43–0.86%) occur in the dark grey layer at 3.9–4.3 rmcd (Fig. 5D).

4. Discussion

4.1. Contribution of higher plant waxes

The major biomarkers in Hole M0004C are long-chain *n*-alkanes, *n*-fatty acids and

n-alkan-1-ols. The average CPI values of these compounds are generally high (3.7-4.9), and the distribution pattern is typical of terrestrial higher plant waxes (Eglinton and Hamilton, 1967; Kvenvolden et al., 1967). This pattern indicates that the OM was derived mainly from fresh higher plant material. This is consistent with previously reported results that higher plant biomarkers are dominant in central Arctic Ocean sediments (e.g., Schubert and Stein, 1997; Belicka et al., 2002).

The other higher plant-derived biomarker is oleanene. Oleanene is an early diagenetic product derived from β-amyrin and tarax-14-en-3β-ol, which are specific to angiosperms (Rullkötter et al., 1994). Because herbs are major angiosperms in polar regions, the oleanene may have derived from herbs.

N-alkan-2-ones, *n*-alkan-2-ols, and the hydroxy fatty acids with the OH group in the α, β, ω or (ω–1) positions, which are common compounds in the study samples, were presumably formed by microbial oxidation of higher plant-derived *n*-alkanes (Arpino et al., 1970) and *n*-fatty acids (Boon et al., 1975) because they exhibit a similar homologous pattern to that of *n*-alkanes and *n*-fatty acids. The presence of these oxidised compounds suggests that higher plant waxes suffered microbial alteration through transportation and/or after deposition.

4.2. Contribution of thermally altered OM

Hopanes are diagenetic products derived from biohopanoids biosynthesised by bacteria (Ourisson et al., 1979). The presence of 17β(H), 21β(H) isomers and the absence of 17α(H),21β(H), 17β(H),21α(H), and 22S isomers of homohopane in the study samples indicate that the thermally altered OM from sedimentary rocks is assigned to the “diagenesis” stage of maturity preceding the oil-generation

"catagenesis" stage (Tissot and Welte, 1984). This maturity is roughly equivalent to the maturity of vitrinite, a coal kerogen (modal R_o% ~ 0.3–0.5%) that is present in surfacial sediments of the Laptev Shelf, supplied by the Lena River (Boucsein and Stein, 2000). Sedimentary rock on land, including coal and coaly shale, was likely eroded by ice or water currents and transported to the study site.

Hopanes show three concentration maxima in MIS-6, MIS-4/5 boundary and MIS-3 (Fig. 5H). All three are associated with IRD maxima (Fig. 5C). The hopane/TOC ratio is significantly correlated ($r = 0.78$, $p < 0.01$) with the IRD (>63 μm) content. This correspondence suggests that the thermally altered OM was transported together with ice rafted debris to the study site.

4.3. Contribution of bacteria

Anteiso- and *iso*-fatty acids are derived from bacteria (Kaneda, 1991). The total concentration of *anteiso*- and *iso*-fatty acids, as normalized on TOC, tends to be higher in samples that have low IRD content (Fig. 5M), reflecting enhanced bacterial activity in the source region during warmer periods. The availability of dissolved organic carbon is a limiting factor for bacterial activity in the Arctic Ocean continental margins (e.g., Laptev Sea, Saliot et al., 1996). Enhanced fluvial discharge, as suggested for the Kara and Laptev Seas by Boucsein et al. (2002), might have increased the bacterial activity in the continental shelf during warmer periods. A warm climate might also have increased bacterial activity in terrestrial soil.

Branched GDGTs are presumably derived from anaerobic bacteria and occur widely in soils and peat bogs (Weijers et al., 2006a). Hopmans et al. (2004) defined the Branched and Isoprenoid Tetraether (BIT) index as the ratio of branched GDGTs to the

sum of branched GDGTs and crenarchaeol as an index of terrestrial soil OM contribution. The BIT index ranges from ~ 0.5 to 1, which is anomalously high for pelagic marine sediments (Fig. 5J). Schouten et al. (2007b) found relatively high BIT index values (~ 0.4–0.6) for late Pleistocene Heinrich layers from the North Atlantic Ocean and interpreted the phenomenon to indicate the transport of soil by ice rafting. These observations suggest that the high BIT index in the central Arctic Ocean reflects a significant contribution of terrestrial soil OM.

4.4. *Contribution of Archaea*

Crenarchaeol in marine sediments is thought to be derived mainly from pelagic crenarchaeota (Sinninghe Damsté et al., 2002b). Weijers et al. (2006b) recently found crenarchaeol in soil samples, some of which have low BIT index values of ~ 0.5. Because the crenarchaeol found in our samples is associated with abundant branched GDGTs, it might have mostly derived from a soil crenarchaeota origin or a mixed origin of soil and aquatic crenarchaeota, although microbiological studies have demonstrated the presence of marine crenarchaeota in Arctic waters (Bano et al., 2004). Caldarchaeol (GDGT-0) is more abundant than crenarchaeol in the study samples (Fig. 4). Caldarchaeol is often more abundant than crenarchaeol in terrestrial soils (Wijers et al., 2006b), which thus suggests the contribution of soil Archaea to central Arctic sediments. In most marine sediments that we have investigated (i.e., Pacific tropical to temperate regions), caldarchaeol is generally less abundant than crenarchaeol (> 800 samples; M. Yamamoto, unpublished data). Because caldarchaeol is a major lipid of some euryarchaeota (Nishihara et al., 1987), some caldarchaeol likely derived from euryarchaeota.

4.5. Contribution of eukaryotic algae

Previous studies found abundant phytoplankton-derived compounds such as polyunsaturated fatty acids, phytol, and dinosterols in sediments from the Arctic along the northern Eurasian and North American margins, especially in estuaries and polynyas (e.g., Yunker et al., 1995, 2005; Peulvé et al., 1996; Zegouagh et al., 1996; Fahl and Stein, 1997, 1999; Belicka et al., 2002, 2004). In contrast, no unambiguous evidence for phytoplankton biomarkers is indicated at the study site. Two mechanisms could have induced this lack of phytoplankton biomarkers. First, severe degradation might reduce marine biomarkers preferentially. Marine biomarkers are generally more labile than terrestrial biomarkers (e.g., Prahl et al., 1997; Sinninghe Damsté et al., 2002a). The sedimentation rate is ~ 2–3 cm/kyr at the study site (Fig. 2). Because of such slow sedimentation in oxygen-rich benthic water, marine biomarkers might suffer preferential degradation, resulting in their absence. Second, low algal production might induce a lack of marine biomarkers. In modern times, the study site in the central Arctic has been permanently ice-covered (e.g., Colony and Thorndike, 1985). Ice algae are primary producers in the area covered by sea ice and production is estimated at ~ 15 $gC/m^2/yr$, much lower than in estuaries and polynyas (Gosselin et al., 1997). Such low algal production might also induce a lack of phytoplankton biomarkers.

Although there is no unambiguous evidence for phytoplankton biomarkers, the presence of short-chain C_{14}–C_{18} *n*-fatty acids and cholesterol suggests some contribution of aquatic organisms (Kvenvolden et al., 1967; Huang and Meinschein, 1979). The abundance ratios of β-sitosterol to cholesterol and of long-chain to short-chain *n*-acids both exhibit a similar trend: relatively high values in MIS-6 (Figs.

5G and 5I), suggesting lower contributions from aquatic organisms in MIS-6.

4.6. Deposition of the dark grey layer

A distinctive dark grey layer was observed in the interval between 3.9 and 4.3 rmcd in ACEX Holes M0003A and M0004C (low L* and low a* in Fig. 5B; Backman et al., 2006). Such a thick layer was not observed in nearby piston cores from the Lomonosov Ridge (e.g., Jakobsson et al., 2001). The thickness of the dark grey layer is ~30 cm in Hole M0003A and ~40 cm in Hole M0004C. The sites of M0003 and M0004 are located at the center of a small basin on the Lomonosov Ridge (Backman et al., 2006). These suggest that the dark grey layer has a lens shape and was thickened by sediment focusing. According to the age–depth model by O'Regan et al. (2008), this dark grey layer dates to early to mid-MIS-6.

Normalized on the TOC, the concentrations of long-chain *n*-alkanes, *n*-fatty acids, and *n*-alkan-1-ols are higher, not only in dark grey layer, but in the whole interval of MIS-6 than in other intervals (Fig. 5E). Other higher plant biomarkers such as β-sitosterol and oleanene show similar trends (Fig. 5I). One of the concentration maxima in MIS-6 is of hopanes (Fig. 5H). Concentrations of branched GDGTs are also higher, normalized on the TOC, in MIS-6 (Fig. 5J). These observations imply that the terrestrial contribution was enhanced in MIS-6.

The dark grey layer is characterised by elevated TOC (0.43–0.86%; Fig. 5D). The elevated TOC in the dark grey layer could not have been a result of better OM preservation because labile compounds such as unsaturated fatty acids are not relatively abundant (Fig. 5N), and phytol and poly-unsaturated fatty acids, which are more labile compounds, are absent. The peak of the branched GDGT concentration normalized on

TOC in the dark grey layer indicates that the layer is more enriched with terrestrial soil OM (Fig. 5J).

IRD records from Sites M0003 and M0004 in the central Arctic demonstrate that IRD numbers are consistently low from 1.8 Ma to MIS-7 and increase after MIS-6 (Sakamoto et al., in preparation). This suggests that MIS-6 was the first period since 1.8 Ma during which the Eurasian Ice Sheet, a potential contributor of IRD to the central Arctic, covered a large area of northern Siberia. According to a reconstruction of the Eurasian Ice Sheet by Svendsen et al. (2004), the eastward expansion of the continental ice sheet was greater during MIS-6 than during the last glacial. The expanded ice sheet eroded terrestrial soil over the West Siberian Lowlands and Central Siberian Mountains. The eroded soil was then transported to the central Arctic by ice rafting, resulting in the deposition of a dark grey layer enriched with terrestrial soil.

Stein et al. (2001) reported the presence of an organic-rich dark grey layer in MIS-6 on the slopes of the Laptev Shelf and the Lomonosov Ridge near the edge of the Laptev Shelf. Their Rock-Eval analysis yielded low hydrogen index (HI) values for the dark grey layer, suggesting an enhanced contribution from terrigenous OM during MIS-6. Although stratigraphic correlation is insufficient to determine the timing of deposition, these observations suggest that the deposition of a dark grey layer was a common phenomenon in MIS-6. Our results highlight a significant terrestrial contribution to this layer in the central Arctic, suggesting that the sedimentary system associated with the layer was not restricted to the Laptev Sea and the adjacent region, but extended to the central Arctic Ocean.

4.7. Changes of terrigenous OM composition after MIS-6 and their relationship to the

glaciation of the Eurasian ice sheet.

The labile–refractory index is defined as the abundance ratio of C_{24}–C_{32} *n*-alkan-1-ols to the sum of C_{25}–C_{35} *n*-alkanes and C_{24}–C_{32} *n*-alkan-1-ols, similar to the definition of the HPA index (Westerhausen et al., 1993). The HPA index is useful for evaluating the proportion of labile and refractory OM in Arctic sediments (Belicka et al., 2004) because *n*-alkan-1-ols are more labile than *n*-alkanes. The labile–refractory index decreases at the MIS-5/6 boundary and continues at lower levels (average 0.61) than those prior to the MIS-5/6 boundary (average 0.80; Fig. 5L). This change suggests that the bulk property of terrigenous OM changed to more refractory at MIS-5/6 boundary.

Hopanes show three concentration maxima in MIS-6, MIS-4/5, and MIS-3, respectively (Fig. 5H). The first maximum in MIS-6 correlates with a maximum in branched GDGT concentration; the last two maxima do not. This suggests that the content of terrestrial soil decreased in terrigenous detrital matter supplied to the central Arctic after MIS-6, implying a decrease in soil cover in the source region.

During MIS-6, the expanded Eurasian Ice Sheet eroded terrestrial soil over the West Siberian Lowlands and Central Siberian Mountains (Svendsen et al., 2004). After the retreat of the ice sheet, soils containing fresh terrestrial OM had been depleted in the source region, which resulted in a relative increase in the contribution of more refractory terrestrial OM to the central Arctic Ocean.

5. Conclusions

Biomarker records from central Arctic sediments show drastic changes with glacial–interglacial contrasts. Concentrations of higher plant-derived compounds, thermally altered compounds, and soil-derived compounds are highly sensitive to past

changes in the environment of the source region. Because the micropaleontological approach is limited in the Arctic Ocean, future investigation of the biomarkers in cores from the central Arctic will help to understand better past climate changes in the polar region.

Acknowledgements

We thank shipboard and shore-based scientists of IODP Expedition 302 and the staff of Bremen Core Repository for sampling. We also thank Ellen Hopmans and Stefan Schouten (Royal Netherlands Institute for Sea Research) for kindly giving us advice about GDGT analysis. Thanks go to Masao Minagawa (Hokkaido University) for help with analysis and Matt O'Regan (University of Rhode Island) and Martin Jakobsson (Stockholm University) for discussions about age–depth models. Special thanks are due to Stefan Schouten, Appy Slijs and an anonymous reviewer for improving this manuscript. The research used samples provided by the Integrated Ocean Drilling Program. This study was supported by a grant-in-aid for Scientific Research (Houga Kenkyu) from the Japan Society for the Promotion of Science, No. 18654089 (MY).

References

Aagaard, K., Carmack, E.C., 1989. The role of sea ice and other fresh water in the Arctic circulation. Journal of Geophysical Research 94, 14485-14498.

Arpino, P., Albrecht, P., Ourisson, G., 1970. Geochimie organique – Series homologues aliphatiques dans un sediment ecocene d'origine lacustre. Comptes Rendus de l'Acdamie des Sciences de Paris 270, 1760-1763.

Backman, J., Moran, K., McInroy, D.B., Mayer, L.A., the Expedition 302 Scientists, 2006. Proceedings of Integrated Ocean Drilling Program, 302. Integrated Ocean Drilling Program Management International, Inc., Edinburgh, doi:10.2204/iodp.proc.302.2006

Bano, N., Ruffin, S, Ransom, B., Hollibaugh, J.T., 2004. Phylogenetic composition of Arctic Ocean Archaeal assemblages and comparison with Antarctic assemblages. Applied and Environmental Microbiology 70, 781-789.

Belicka, L.L., Macdonald, R.W., Harvey, H.R., 2002. Sources and transport of organic carbon to shelf, slope, and basin surface sediments of the Arctic Ocean. Deep-Sea Research I 49, 1463-1483.

Belicka, L.L., Macdonald, R.W., Yunker, M.B., Harvey, H.R., 2004. The role of depositional regime on carbon transport and preservation in Arctic Ocean sediments. Marine Chemistry 86, 65-88.

Boon, J.J., de Leeuw, J.W., Schenck, P.A., 1975. Organic geochemistry of Walvis Bay diatomaceous ooze-I. Occurrence and significance of the fatty acids. Geochimica et Cosmochimica Acta 39, 1559-1565.

Boucsein, B., Stein, R., 2000. Particulate organic matter in surface sediments of the Laptev Sea (Arctic Ocean): application of maceral analysis as organic-carbon-source indicator. Marine Geology 162, 573-586.

Bouscein, B., Knies, J., Stein, R., 2002. Organic matter deposition along the Kara and Laptev Seas continental margin (eastern Arctic Ocean) during the last deglaciation and Holocene: evidence from organic-geochemical and petrographic data. Marine Geology 183, 67-87.

Bray, E.E., Evans, E.D., 1961. Distribution of n-paraffins as a clue to recognition of

source beds. Geochimica et Cosmochimica Acta 22, 2-15.

Broecker, W.S., 1991. The great ocean conveyor belt. Oceanography 4, 79-89.

Colony, R., Thorndike, A.S., 1985. Sea ice motion as a drunkard's walk. Journal of Geophysical Research C90, 965-974.

Darby, D.A., Bischop, J.F., Spielhagen, R.F., Marshall, S.A., Herman, S.W., 2002. Arctic ice export events and their potential impact on global climate during the late Pleistocene. Paleoceanography 17, 15-1-17.

Eglinton, G., Hamilton, R.J., 1967. Leaf epicuticular waxes. Science 156, 1322-1355.

Fahl, K., Stein, R., 1997. Modern organic carbon deposition in the Laptev Sea and the adjacent continental slope: surface water productivity vs. terrigenous input. Organic Geochemistry 26, 379-390.

Fahl, K., Stein, R., 1999. Biomarkers as organic-carbon-source and environmental indicators in the Late Quaternary Arctic Ocean: problems and perspectives. Marine Chemistry 63, 293-309.

Fütterer, D.K., 1992. ARCTIC '91: The expedition ARK-VIII/3 of RV "Polarstern" in 1991. Ber. z. Polarforsch. 107, 1-267.

Gordienko, P.A., Laktionov, A.F., 1969. Circulation and physics of the Arctic Basin waters. Annals of International Geophysical Year, Oceanography 46, 94-112.

Gosselin, M., Levasseur, M., Wheeler, P.A., Horner, R.A., Booth, B.C., 1997. New measurements of phytoplankton and ice algal production in the Arctic Ocean. Deep-Sea Research II 44, 1623-1644.

Grosjean, E., Logan, G.A., 2007. Incorporation of organic contaminants into geochemical samples and an assessment of potential sources: Examples from Geoscience Australia marine survey S282. Organic Geochemistry 38, 853-869.

Hopmans, E.C., Schouten, S., Pancost, R., van der Meer, M.T.J., Sinninghe Damsté, J.S., 2000. Analysis of intact tetraether lipids in archaeal cell material and sediments by high performance liquid chromatography/atmospheric pressure chemical ionization mass spectrometry. Rapid Communications in Mass Spectrometry 14, 585-589.

Hopmans, E.C., Weijers, J.W.H., Schefuss, E., Herfort, L., Sinninghe Damsté, J.S., Schouten, S., 2004. A novel proxy for terrestrial organic matter in sediments normalized on branched and isoprenoid tetraether lipids. Earth and Planetary Science Letters 224, 107-116.

Huang, W.-Y., Meinschein, W.G., 1979. Sterols as ecological indicators. Geochimica et Cosmochimica Acta 43, 739-745.

Jakobsson, M., Løvlie, R., Arnold, E.A., Backman, J., Polyak, L., Knutsen, J.-O., Musatov, E., 2001. Pleistocene stratigraphy and paleoenvironmental variation from Lomonosov Ridge sediments, central Arctic Ocean. Global and Planetary Change 31, 1-22.

Kaneda, T., 1991. Iso- and anteiso-fatty acids in bacteria: biosynthesis, function, and taxonomic significance. Microbiological Reviews 55, 288-302.

Kenig, F., Simons, D.H., Crich, D., Cowen, J.P., Ventura, G.T., Rehbein-Khalily, T., Brown, T.C., Anderson, K.B., 2003. Branched aliphatic alkanes with quaternary substituted carbon atoms in modern and ancient geologic samples. Proceeding of the Natural Academy of Sciences 100, 12554-12558.

Kvenvolden, K.A., 1967. Normal fatty acids in sediments. Journal of the American Oil Chemists' Society 44, 628-636.

Langereis, C.G., Dekkers, M.J., de Lange, G.J., Paterne, M., van Santvoort, P.J.M., 1997. Magnetostratigraphy and astronomical calibration of the last 1.1 Ma from an eastern

Mediterranean piston core and dating of short events in the Brunhes. Geophysical Journal International 129, 75–94.

Nishihara, M., Horii, H., Koga, Y., 1987. Structure determination of a quartet of novel tetraether lipids from *Methanobacterium thermoautotrophicum*. Journal of Biochemistry 101, 1007-1015.

Nowaczyk, N.R., Frederichs, T.W., 1999. Geomagnetic events and relative palaeointensity variations during the past 300 ka as recorded in Kolbeinsey Ridge sediments, Iceland Sea: indication for a strongly variable geomagnetic field. International Journal of Earth Sciences 88,116-131.

Nürnberg, D., Wollenburg, I., Dethleff, D., Eicken, H. Kassens, H., Letzig, T., Reimnitz, E., Thiede, J., 1994. Sediments in Arctic sea ice: Implications for entrainment, transport and release. Marine Geology 119, 185-214.

O'Regan, M., King, J., Backman, J., Jakobsson, M., Pälike, H., Moran, K., Heil, C., Sakamoto, T., Cronin, T., Jordan, R.W., 2008. Constraints on the Plio-Pleistocene Chronology of Sediments from the Lomonosov Ridge. Paleoceanography, in press. doi:10.1029/2007PA001551

Ourisson, G., Albrecht, P., Rohmer, M., 1979. The hopanoids: Paleochemistry and biochemistry of a group of natural products. Pure and Applied Chemistry 51, 709-729.

Peulvé, S., Sicre, M.-A., Saliot, A, de Leeuw, J.W., Baas, M., 1996. Molecular characterization of suspended and sedimentary organic matter in an Arctic delta. Limnology and Oceanography 41, 488-497.

Prahl, F.G., de Lange, G.J., Sholten, S., Cowie, G.L., 1997. A case of post-depositional aerobic degradation of terrestrial organic matter in tubidite deposits from the Madeira

Abyssal Plain. Organic Geochemistry 27, 141-152.

Rullkötter, J., Peakman, T.M., ten Haven, H.L., 1994. Early diagenesis of terrigenous triterpenoids and its implications for petroleum geochemistry. Organic Geochemistry 21, 215-233.

Sakamoto T., Sugisaki. S., Iijima K., Yamamoto M., O'Regan M., King J., High-resolution reconstruction of the Arctic-ice history and origin of Mn-rich brown color layers during 2 Ma in the central Arctic Ocean (IODP Expedition 302: ACEX) by non-destructive sediment-scanning techniques, TATSCANs. in preparation.

Saliot, A., Cauwet, G. Cahet, G., Mazaudier, D., Daumas, R., 1996. Microbial activities in the Lena River delta and Laptev Sea. Marine Chemistry 53, 247-254.

Schouten, S, Hopmans, E.C., Scefuß, E., Sinninghe Damsté, J.S., 2002. Distributional variations in marine crenarchaeotal membrane lipids: a new tool for reconstructing ancient sea water temperatures? Earth and Planetary Letters 204, 265-274.

Schouten, S, Hudget, C., Hopmans, E.C., Kienhuis, M.V.M., Sinninghe Damsté, J.S., 2007a. Analytical methodology for TEX_{86} paleothermometry by high performance liquid chromatography/atmospheric pressure chemical ionization-mass spectrometry. Analytical Chemistry 79, 2940-2944.

Schouten, S, Ossebaar, J., Brummer, G.J., Elderfield. H., Sinninghe Damsté, J.S., 2007b. Transport of terrestrial organic matter to the deep North Atlantic Ocean by ice rafting. Organic Geochemistry 38, 1161-1168.

Schubert, C.J., Stein, R., 1996. Deposition of organic carbon in Arctic sediments: terrigenous supply vs marine productivity. Organic Geochemistry 24, 421-436.

Schubert, C.J., Stein, R., 1997. Lipid distribution in surface sediments from the eastern central Arctic Ocean. Marine Geology 138, 11-25.

Sinninghe Damsté, J.S., Rijpstra, W.I., Reichart, G.-J., 2002a. The influence of oxic degradation on the sedimentary biomarker record II. Evidence from Arabian Sea sediments. Geochimica et Cosmochimica Acta 66, 2737–2754.

Sinninghe Damsté, J.S., Schouten, S., Hopmans, E.C., van Duin, A.C.T., Geenevasen, J.A.J., 2002b. Crenarchaol: the characteristic core glycerol dibiphytanyl glycerol tetraether membrane lipid of cosmopolitan pelagic crenarchaeota. Journal of Lipid Research 43, 1641-1651.

Spielhagen, R.F., Baumann, K.-H., Erlenkeuser, H., Nowaczyk, N.R., Nørgaard-Pedersen, N., Vogt, C., Weiel, D., 2004. Arctic Ocean deep-sea record of northern Eurasian ice sheet history. Quaternary Science Reviews 23, 1455-1483.

Stein, R., Grobe, H., Wahsner, M., 1994. Organic carbon, carbonate, and clay mineral distributions in eastern central Arctic Ocean surface sediments. Marine Geology 119, 269-285.

Stein, R., Boucsein, B., Fahl, K., de Oteyza, T.G., Niessen, K.F., 2001. Accumulation of particulate organic carbon at the Eurasian continental margin during late Quaternary times: controlling mechanisms and paleoenvironmental significance. Global and Planetary Change 31, 87-104.

Stein, R., Dittmers, K., Fahl, K., Kraus, M., Matthiessen, J., Niessen, F., Pirrung, M., Polyakova, Y., Schoster, F., Steinke, T., Fütterer, D.K., 2004. Arctic (paleo) river discharge and environmental change: evidence from the Holocene Kara Sea sedimentary record. Quaternary Science Reviews 23, 1485-1511.

Svendsen, J.I., Alexanderson, H., Astakhov, V.I., Demidov, I., Dowdeswell, J.A., et al., 2004. Late Quaternary ice sheet history of northern Eurasia. Quaternary Science Reviews 23, 1229-1271.

Tissot, B.P. and Welte, D.H., 1984. *Petroleum Formation and Occurrence*, 2nd. ed., Springer-Verlag, Berlin.

Weijers, J.W.H., Schouten, S., Hopmans, E.C., Geenevasen, J.A.J., David, O.R.P., Coleman, J.M., Pancost, R.D., Sinninghe Damsté, J.S., 2006a. Membrane lipids of mesophilic anaerobic bacteria thriving in peats have typical archaeal traits. Environmental Microbiology 8, 648-657.

Weijers, J. W. H., Schouten, S., Spaargaren, O.C., Sinninghe Damsté, J.S., 2006b. Occurrence and distribution of tetraether membrane lipids in soils: Implications for the use of the TEX_{86} proxy and the BIT index. Organic Geochemistry 37, 1680-1693.

Westerhausen, L., Poynter, J., Eglinton, G., Erlenkeuser, H., Sarnthein, M., 1993. Marine and terrigenous origin of organic matter in modern sediments of the equatorial East Atlantic: the $\delta^{13}C$ and molecular record. Deep-Sea Research I 40, 1087-1121.

Yunker, M.B., Macdonald, R.W., Veltkamp, D.J., Cretney, W.J., 1995. Terrestrial and marine biomarkers in a seasonally ice-covered Arctic estuary – integration of multivariate and biomarker approaches. Marine Chemistry 49, 1-50.

Yunker, M.B., Belicka, L.L., Harvey, H.R., Macdonald, R.W., 2005. Tracing the inputs and fate of marine and terrigenous organic matter in Arctic Ocean sediments: A multivariate analysis of lipid biomarkers. Deep-Sea Research II 52, 3478-3508.

Zegouagh, Y., Derenne, S., Largeau, C., Saliot, A., 1996. Organic matter sources and early diagenetic alterations in Arctic surface sediments (Lena River delta and Laptev Sea, Eastern Siberia)-I. Analysis of the carboxylic acids released via sequential treatments. Organic Geochemistry 24, 841-857.

Figure captions

Fig. 1. Location of study site (Backman et al., 2006) and the bathymetry and surface currents of the Arctic Ocean.

Fig. 2. Age–depth model of ACEX holes (Modified after O'Regan et al., 2008).

Fig. 3. Gas chromatograms of (A) F1, (B) F4-1, and (C) F4-2 fractions in Sample 302-M0004C-1H-1, 10-12 cm (0.10–0.12 rmcd). Numbers indicate carbon numbers. IS is an internal standard (n-$C_{24}D_{50}$).

Fig. 4. The HPLC/MS base peak of tetraether lipids in the F4 fraction of Sample 302-M0004C-2H-1, 76-78 cm (4.10–4.12 rmcd).

Fig. 5. Depth variations in (A) age, (B) colour reflectance (L* and a*; Backman et al., 2006), (C) IRD content (> 1mm and > 63 μm particles; Sakamoto et al., in preparation), (D) TOC content, (E) concentrations of long-chain C_{25}-C_{35} *n*-alkanes, C_{24}-C_{32} *n*-fatty acids and C_{24}-C_{32} *n*-alkan-1-ols normalized on TOC, (F) carbon number preference index (CPI), (G) ratio of long-chain C_{24}-C_{32} to short-chain C_{14}-C_{18} *n*-fatty acids, (H) concentrations of oleanenes (Δ^{12} + Δ^{18}) and C_{29}-C_{31} hopanes, (I) concentrations of cholesterol and β-sitosterol and their abundance ratio, (J) concentrations of branched and isoprenoid GDGTs and the branched and isoprenoid tetraether (BIT) index, (K) concentrations of caldarchaeol and crenarchaeol and their abundance ratio, (L) labile–refractory index (the abundance ratio of C_{24}–C_{32} *n*-alkan-1-ols to the sum of

C_{25}–C_{35} *n*-alkanes and C_{24}–C_{32} *n*-alkan-1-ols), (M) concentration of *anteiso*- and *iso*-C_{15} and C_{17} fatty acids, and (N) ratios of *n*-$C_{16:1}$ acid to *n*- $C_{16:0}$ acid (16:1/16:0) and of *n*-$C_{18:1}$ and *n*-$C_{16:2}$ acid to *n*- $C_{18:0}$ acid (18:1/16:0 and 18:2/18:0) in Hole M0004C. The grey band indicates the dark gray layer.

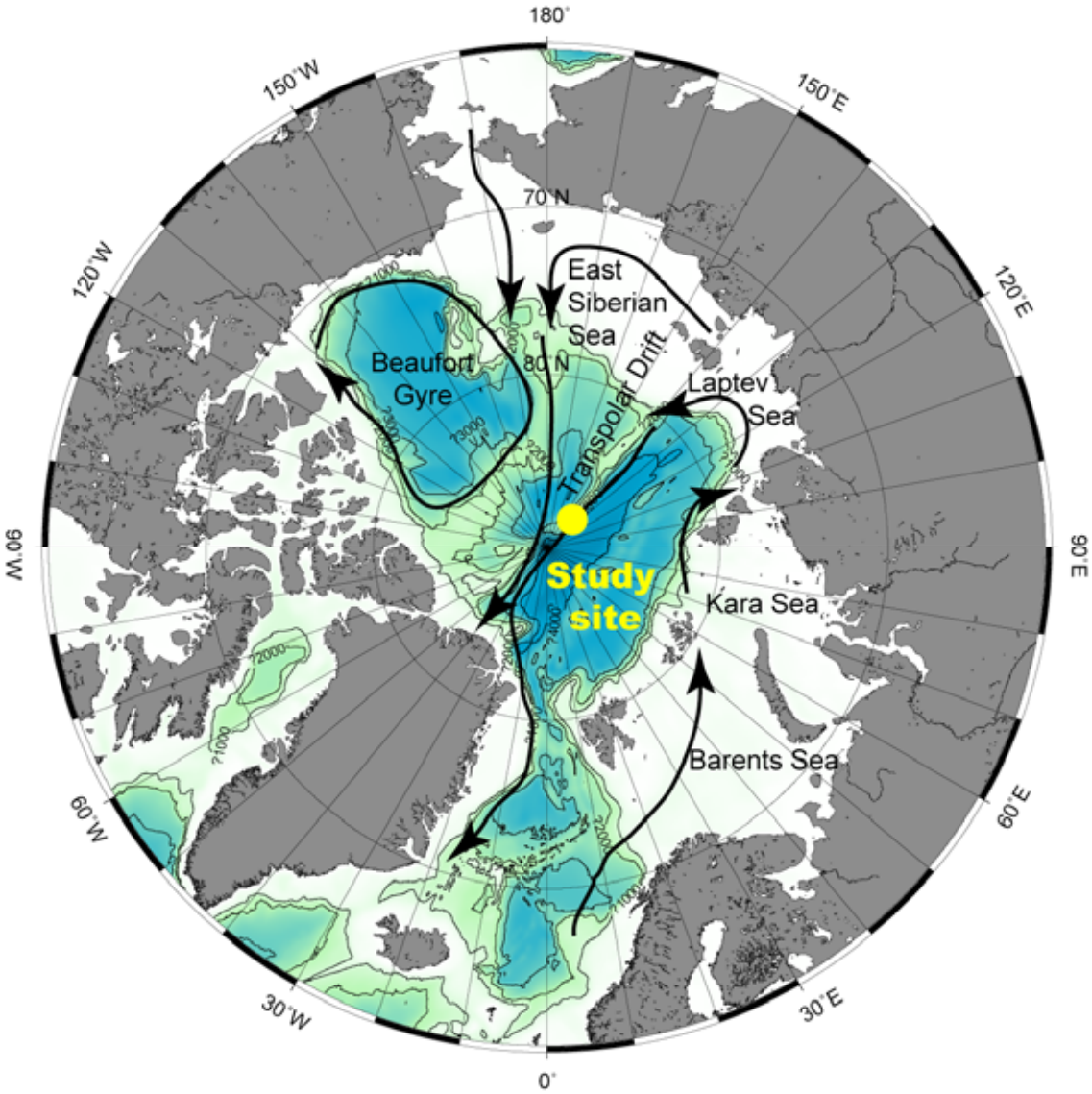
180°
150°W
150°E
120°W
120°E
90°W
90°E
60°W
60°E
30°W
30°E
0°
70°N
80°N
East
Siberian
Sea
Beaufort
Gyre
Transpolar Drift
Laptev
Sea
Study
site
Kara Sea
Barents Sea

Fig. 1

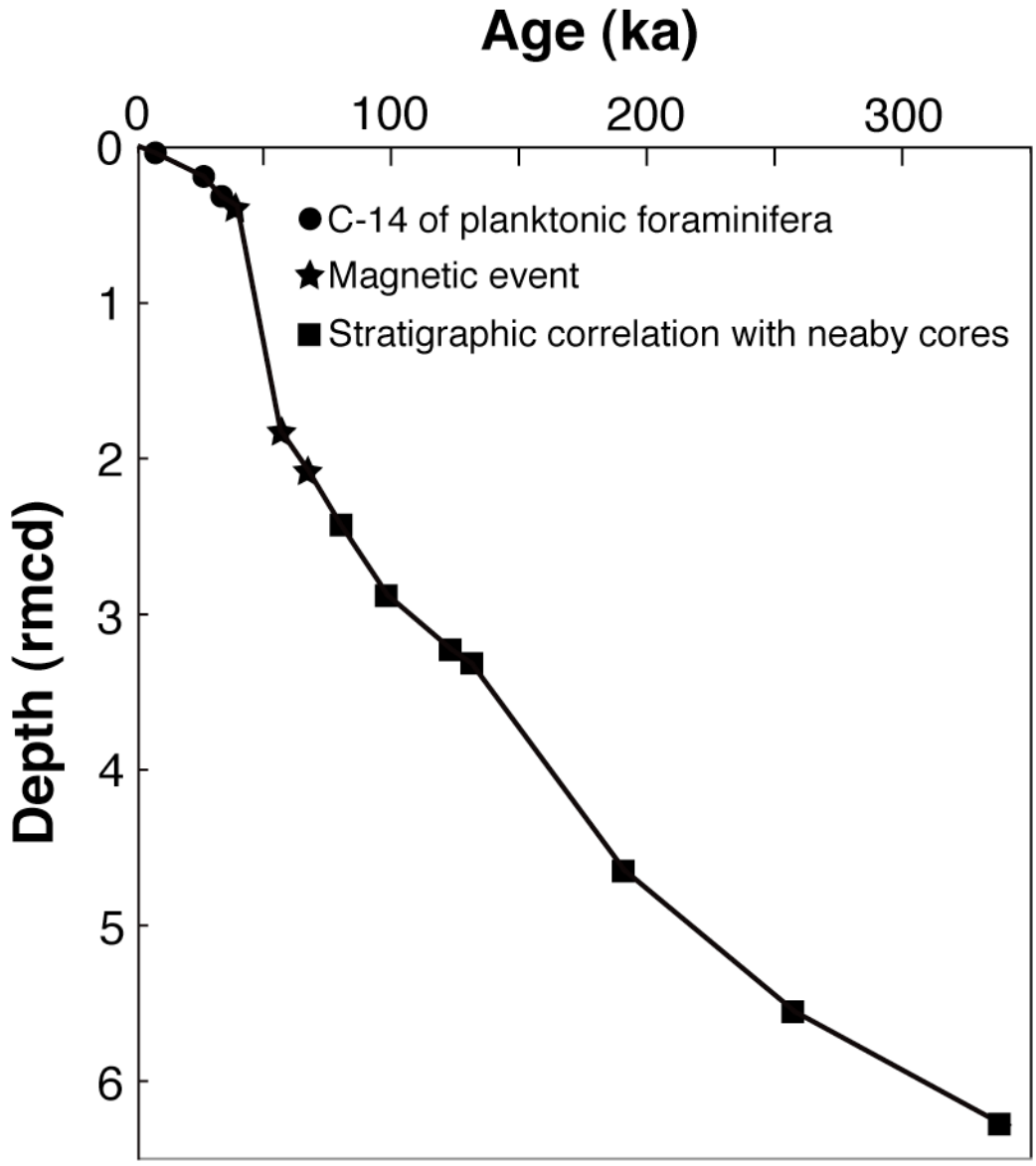
Age (ka)
0
100
200
300
0
1
2
3
4
5
6
Depth (rmcd)
C-14 of planktonic foraminifera
Magnetic event
Stratigraphic correlation with neaby cores

Fig. 2

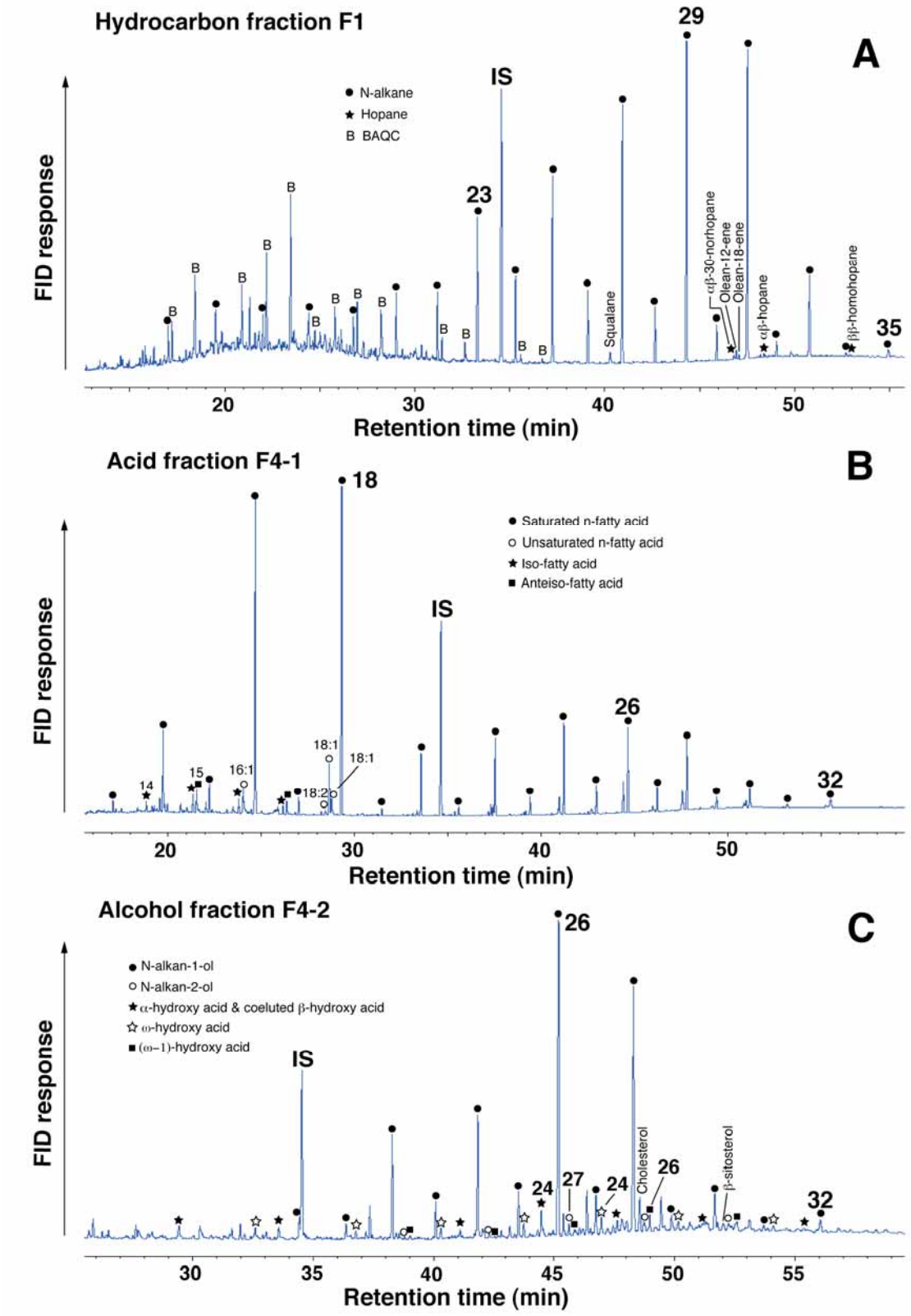
Hydrocarbon fraction F1
A
FID response
N-alkane
Hopane
B BAQC
IS
23
29
35
Squalane
αβ-30-norhopane
Olean-12-ene
Olean-18-ene
αβ-hopane
ββ-homohopene
Retention time (min)
Acid fraction F4-1
B
Saturated n-fatty acid
Unsaturated n-fatty acid
Iso-fatty acid
Anteiso-fatty acid
18
IS
26
32
14
15
16:1
18:1
18:1
18:2
Retention time (min)
Alcohol fraction F4-2
C
N-alkan-1-ol
N-alkan-2-ol
α-hydroxy acid & coeluted β-hydroxy acid
ω-hydroxy acid
(ω−1)-hydroxy acid
IS
26
Cholesterol
β-sitosterol
24
27
24
26
32
Retention time (min)

Fig. 3

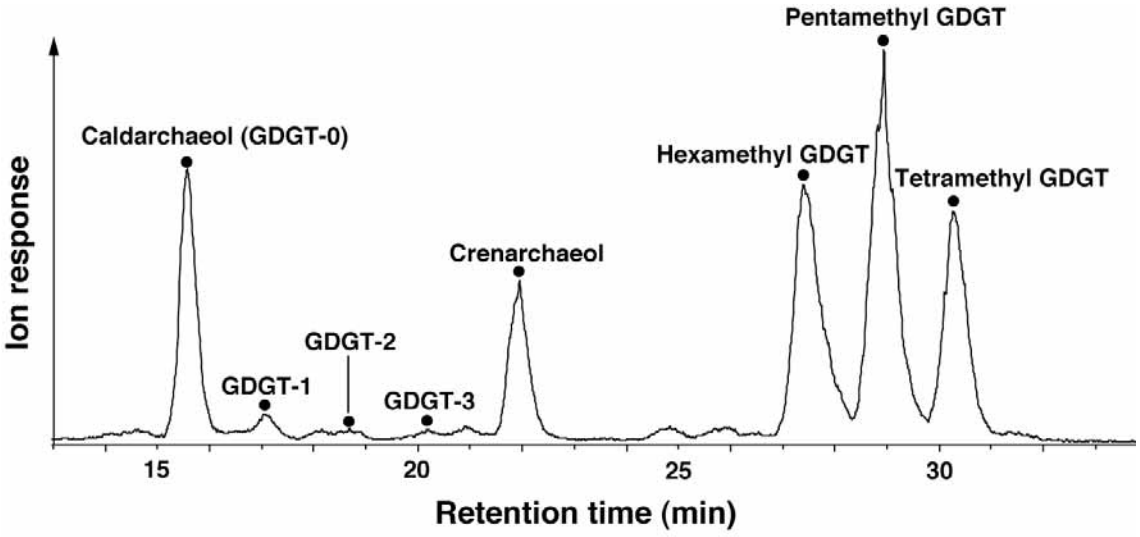
Pentamethyl GDGT
Caldarchaeol (GDGT-0)
Hexamethyl GDGT
Tetramethyl GDGT
Crenarchaeol
GDGT-2
GDGT-1
GDGT-3
Ion response
15
20
25
30
Retention time (min)

Fig. 4

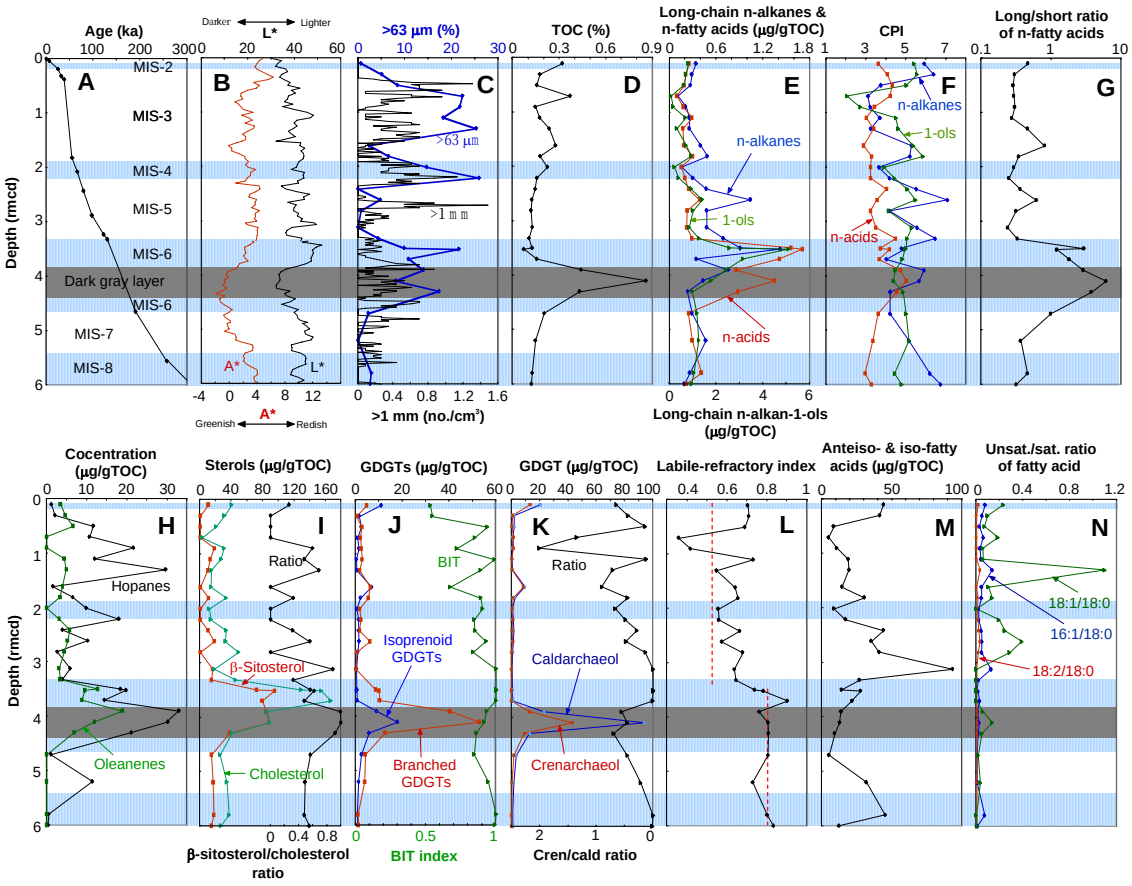
Age (ka)
Darker
L*
Lighter
>63 µm (%)
TOC (%)
Long-chain n-alkanes & n-fatty acids (µg/gTOC)
CPI
Long/short ratio of n-fatty acids
Depth (rmcd)
MIS-2
MIS-3
MIS-4
MIS-5
MIS-6
Dark gray layer
MIS-6
MIS-7
MIS-8
A
B
C
D
E
F
G
A*
L*
Greenish
A*
Redish
>63 µm
>1 mm
n-alkanes
1-ols
n-acids
>1 mm (no./cm³)
Long-chain n-alkan-1-ols (µg/gTOC)
Cocentration (µg/gTOC)
Sterols (µg/gTOC)
GDGTs (µg/gTOC)
GDGT (µg/gTOC)
Labile-refractory index
Anteiso- & iso-fatty acids (µg/gTOC)
Unsat./sat. ratio of fatty acid
H
I
J
K
L
M
N
Hopanes
Oleanenes
Ratio
β-Sitosterol
Cholesterol
BIT
Isoprenoid GDGTs
Branched GDGTs
Ratio
Caldarchaeol
Crenarchaeol
18:1/18:0
16:1/18:0
18:2/18:0
β-sitosterol/cholesterol ratio
BIT index
Cren/cald ratio

Fig. 5